Spaced measurements and progress in understanding space plasma waves*

P. M. Kintner,[†] P. W. Schuck, and J. R. Franz
School of Electrical Engineering, Cornell University, Ithaca, New York 14853

Measuring plasma wave properties with spatially separated antennae observes wavelength, propagation speed, and direction as well as frequency. This approach has been pivotal to progress in understanding three phenomena in space plasmas. The first is lower hybrid solitary waves, which are waves with cylindrical symmetry propagating inside a density cavity. The second is electron phase-space holes, which are propagating vortices in phase space. The third is called broadband ELF (extra low frequency) electric fields and is an important but poorly understood wave process essential to transverse ion acceleration. © *2000 American Institute of Physics.* [S1070-664X(00)91205-9]

I. INTRODUCTION

Despite nearly three decades of plasma wave electric field measurements in space, much of the interpretation of *in situ* measurements focuses on infinite plane waves with wavelengths large compared to the receiving antenna. These plasma wave modes are primarily electromagnetic modes. The issues of electrostatic modes with wavelengths comparable to antenna lengths, modes which exist in inhomogeneous plasmas, and nonlinear structures which cannot be described by infinite plane waves have received less attention. One way of examining these issues is to use spaced antennae, which can investigate wavelengths, propagation directions, and propagation speeds, and use the entire wave form instead of just the power spectrum, which intrinsically neglects half of the information in a Fourier transform—namely, the phase spectrum. During the past decade, spaced electric field measurements in the form of plasma wave interferometers[1] have been included on several sounding rocket experiments as well as the Polar and FAST (Fast Auroral Snapshot) satellites. In this brief overview we examine three areas in which plasma wave interferometers have been crucial for our understanding.

The first phenomenon has several names, but we will call them lower hybrid solitary structures. These long-lived structures are organized around cylindrical density cavities and are solitary only in space. They are excited externally, and the resonant modes have cylindrical symmetry near the lower hybrid frequency. In the steady state they are linear structures, but we do not know how they were originally formed. The second phenomenon we will refer to as electron phase-space holes. These are vortices in velocity space with spatial sizes the order of a Debye length. They move at a fraction of the electron thermal speed and are found in multiple regions of the magnetosphere and perhaps outside the magnetosphere. Their recent discovery by so many spacecraft suggests that electron phase-space holes may be an im-

portant feature of planetary magnetospheres and may explain the well-known phenomenon of broadband electrostatic noise. The last plasma wave phenomenon investigated is called broadband ELF (extra low frequency) electric fields, or BB-ELF for short, and it is the phenomenon about which we know the least. It has no spectral features, although it exists in the range of ionospheric cyclotron frequencies, and it is very closely associated with transverse ion acceleration. In this paper we demonstrate the use of the coherency observable to determine the BB-ELF wavelength.

II. LOWER HYBRID SOLITARY STRUCTURES

Lower hybrid solitary structures (LHSS) are isolated regions of lower hybrid waves localized in field-aligned cylindrical plasma density depletions. The radius of the density depletion is typically larger than the thermal O^+ gyroradius and smaller than the electromagnetic skin depth c/ω_{pe}. The LHSS are always observed embedded in a ubiquitous background of auroral hiss produced by ''inverted-V'' arc electron precipitation. The auroral hiss consists of waves propagating on the whistler lower hybrid-magnetosonic branch of the cold plasma dispersion surface over a frequency band of a few to several hundred kHz. The auroral hiss emission is quasielectrostatic near the lower hybrid resonance $\omega_R = \omega_i/\sqrt{1+\omega_e^2/\Omega_e^2}$, and the power is severely attenuated (cut off) below the lower hybrid resonance.

Observations of LHSS by seven sounding rockets[2–12] and at least two satellites[13–19] encompass an altitude range of 300–14 000 km. The vast number of events recorded indicate that this phenomenon is a common occurrence in the nightside auroral ionosphere. At lower altitudes, sounding rockets have observed LHSS coincident with transversely accelerated ions.[3–6,9,12] Consequently, LHSS may contribute to the total outflow of heavy ions from the auroral ionosphere, although the principal source appears to be BB-ELF waves, discussed in Sec. IV. The most dramatic result of the sounding rocket observations is the observation that LHSS consist of electrostatic wave modes which rotate about the geomagnetic fields in a right-handed sense above the ambi-

ent lower hybrid resonance (LHR) and in a left-handed sense below the LHR. The sounding rocket experiments are equipped with an electric field interferometer comprised of two spatially separated electric field antennae, henceforth labeled ''1'' and ''2.'' LHSS appear as transient bursts in the sounding rocket data because the structures are spatially localized in the plasma rest frame. Consequently, the data are analyzed using wavelet spectral methods, which are aptly suited for transient phenomena.

Figure 1 is the logarithmic color scale representation of the wavelet estimated local frequency wave number spectrum or $P_l(f, K_{12})$, where f is the frequency, $K_{12} = \Delta\phi/(2\pi d)$ in m^{-1} is the projection of the wave vector onto the interferometer axis, and d is the distance between the interferometer centers.[9–11] The abscissa is inverse scale length K_{12} from -0.175 to $0.175\,m^{-1}$, which corresponds to the phase shift of $\Delta\phi$ from $-\pi$ to π of the wavelet cross spectrum of the two antennae. The ordinate is a logarithmic frequency scale four octaves wide from 1.25 to 20.0 kHz. The vertical dashed white line separates positive and negative values of K_{12}. The horizontal dashed white line indicates the value of the ambient LHR. The local frequency wave number spectrum is a power-weighted histogram of the phase shift between the two antennae. The color scale represents the amount of power at a particular scale length and frequency. The local frequency wave number spectrum can be loosely interpreted as the local dispersion relation for the LHSS.

The top panel is the spectrum corresponding to 20 ms centered on the LHSS. The spectrum is roughly symmetrical about zero wave number $K_{12} = 0$. The LHSS was composed of two wave packets with antiparallel phase velocities in each of two frequency bands: one below the ambient LHR at 1.8 kHz and one above the ambient LHR at 4 kHz. At 1.8 kHz the two packets have the characteristic scale lengths of $1/K_{12} = \pm 50$ m, and at 4 kHz the two packets have characteristic scale lengths of $1/K_{12} = \pm 25$ m. The sign of the characteristic scale length indicates the direction of the phase velocity across the 1–2 interferometer (positive for $1 \rightarrow 2$ and negative for $2 \rightarrow 1$). The middle and bottom panels of Fig. 1 are the spectra obtained from the first and second half of the LHSS data, respectively. Figure 1 demonstrates unambiguously that the parallel and antiparallel phase velocity components in each frequency band *do not exist simultaneously* during the LHSS. However, the negative phase velocities at 1.8 kHz exist simultaneously with the positive phase velocities at 4 kHz, and the positive phase velocities at 1.8 kHz exist simultaneously with the negative phase velocities at 4 kHz. Using the direction of the geomagnetic field with respect to the interferometer axis, this analysis demonstrates that the LHSS is unequivocally composed of right-hand rotating waves above the LHR and left-hand rotating waves below the LHR.[11]

The rotation of wave modes in a cylindrical density profile is a result of the geometry. Lower hybrid waves localized within a cylindrical density profile are nondegenerate due to the vector nature of the Hall current which governs the interaction. At frequencies near the LHR, ions respond in the direction of the electric field, whereas electrons **E×B** drift.
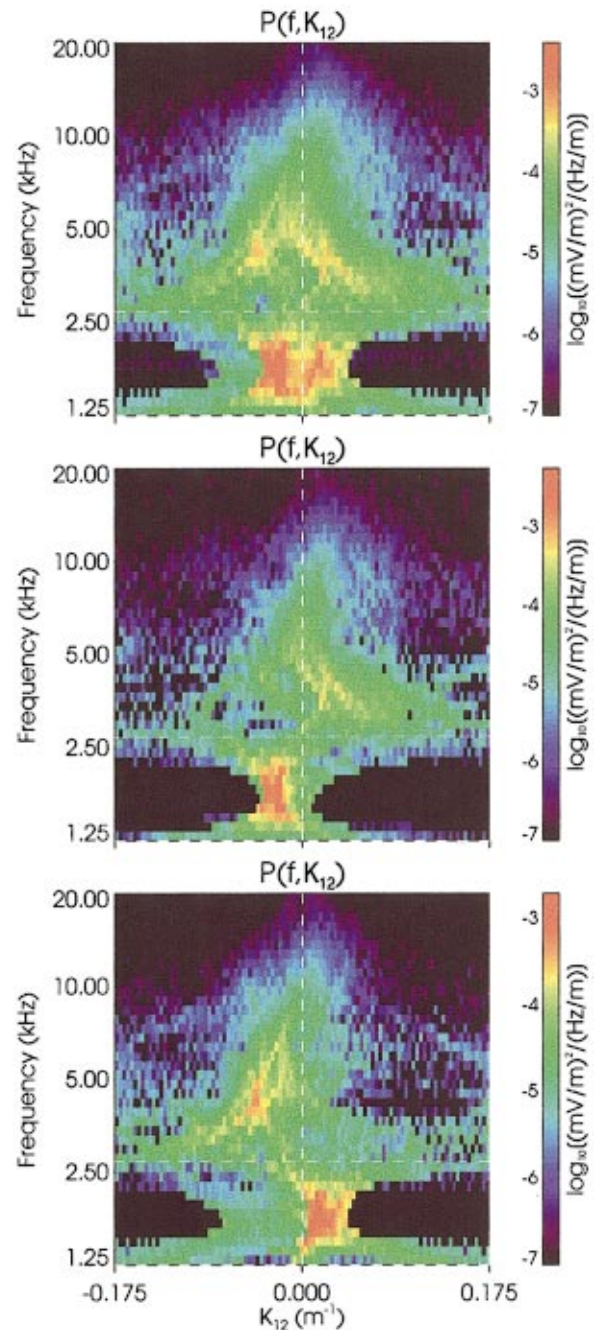

FIG. 1. (Color) Logarithmic color scale representation of the local frequency wave number spectrum for the LHSS. Frequency is on a logarithmic scale, and inverse length K_{12} is on a linear scale. The vertical dashed white line separates positive and negative values of K_{12}. (Top) spectrum corresponding to 20 ms centered on the LHSS. (Middle, bottom) spectra obtained from the first and second half of the data, respectively. From Bonnell *et al.*, Ref. 11. Used by permission of the American Physical Society.

The Hall current carried by the electrons is obviously not in the direction of the electric field (hence the interaction is manifestly vectorial). In a homogeneous plasma the Hall current is divergence free and does not contribute to the propagation characteristics of lower hybrid waves. However, when the electron **E×B** drift is parallel to a density gradient, the Hall current is not divergence free, significantly modifying the propagation characteristics of lower hybrid waves.

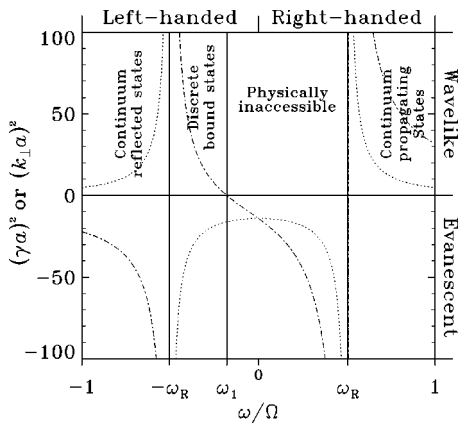For a finite-range cylindrical density depletion, radius a,

FIG. 2. The function $\gamma^2(\omega)$ for $r<a$ (dotted-dashed line) and $k_\perp^2(\omega)$ for $r>a$ (dotted line) for $\Delta=-0.35$, $a=2.5\rho_s$, $m_i k_z/m_e=1.5\pi$, $m=1$, and $\omega_R=\omega_{LH}$. Right-handed modes have $\omega>0$, and left-handed modes have $\omega<0$. From Schuck et $al.$, Ref. 10, copyright by the American Geophysical Union. Used by permission of the American Geophysical Union.

FIG. 3. 40 ms of Polar electric field measurements.

and depth $\delta n/n_0 \equiv \Delta$, the wave modes are described by rotating states of the form $\varphi \propto \hat{R}_m(r) e^{i(m\theta+k_z z-\omega t)}$. Figure 2 shows the local dispersion relations for the radial wave vectors $k_\perp^2(\omega)$ for $r>a$ (dotted line) and $\gamma^2(\omega)$ for $r<a$ (dot-dashed line) for the $m=1$ azimuthal eigenstates. Right-handed waves have $\omega>0$ and left-handed waves have $\omega<0$. When the radial wave vector is greater than zero, the mode propagates, and when the radial wave vector is less than zero, the mode is below cutoff and evanesces. The dispersion relation outside the finite-range density profile is the homogeneous lower hybrid dispersion relation: propagating for frequencies above the LHR and evanescent for frequencies below. Right-handed and left-handed lower hybrid waves are degenerate in the homogeneous plasma outside the finite-range density depletion. However, within the density depletion, the behavior is quite different. Left-handed waves above the LHR evanesce within the density depletion, but propagate below the LHR. Right-handed waves above the LHR can propagate within the density depletion and evanesce below the LHR. Clearly the density depletion breaks the degeneracy between right- and left-handed waves. Left-handed waves above the LHR are reflected from the density depletion. Left-handed waves below the LHR are trapped in the density profile and are bound states under the electrostatic approximation. Right-handed waves above the LHR can propagate inside the density profile. Consequently, a sounding rocket passing through the density depletion should observe right-handed waves above the LHR and left-handed waves below the LHR. This is precisely what is observed by the sounding rocket experiments.

III. ELECTRON PHASE-SPACE HOLES IN THE MAGNETOSPHERE

In this section we discuss observations of electron phase-space holes by the Polar plasma wave instrument.[20] The orbit of the Polar spacecraft has a 90° inclination, a perigee of 5100 km, and an apogee of about 51 000 km. During high altitude (25 000 to 45 000 km) passes through the polar mag-
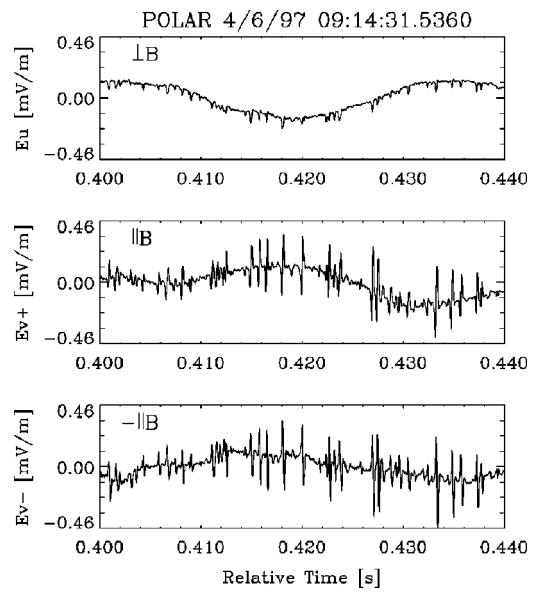
netosphere, wave electric field detectors respond to coherent electrostatic structures.[21,22] Similar structures have been observed in many different regions of the magnetosphere, including the magnetotail,[23,24] the bow shock,[25,26] the solar wind,[27] and the auroral acceleration region.[28–31] Thus, the structures are observed in a wide range of plasma environments covering $\beta \ll 1$ to $\beta \approx 1$.

Figure 3 presents 40 ms of electric field wave form data from a time period when the spacecraft was in the high altitude ($\approx 41\,000$ km) cusp. The top panel contains the wave form from the Eu antenna, which was perpendicular to **B** at this time. The second and third panels contain the wave forms from the Ev+ and Ev− antennae, which were about 30° from **B**. The Ev+ and Ev− antennae are collinear and comprise a plasma wave interferometer. In Fig. 3 the most obvious wave features are the coherent structures. Notice that the signatures of the structures are bipolar in the parallel direction and unipolar in the perpendicular direction.

An interpretation consistent with the observations is that the structures are unipolar electrostatic potentials propagating parallel to **B**. The opposite polarities of the structures in the Ev+ and Ev− antennae are simply the result of the opposite polarity of the antennae. Using a cross-correlation analysis on the interferometer data, we have determined that the structures correspond to positive potential pulses propagating along **B** at velocities the order of (although often less than) the electron thermal velocity. Typical parallel scale sizes for the structures are the order of the Debye length, which is about 24 m in this region of space ($T_e \approx 20$ eV and $n_e \approx 2$ cm^{-3}). Furthermore, the larger amplitude structures tend to have larger scale sizes than the smaller amplitude structures, contrary to theoretical predictions for solitons.

There are two additional features illustrated in Fig. 3 that should be noted. First, the magnitude of $E_\perp$ is significantly smaller than the magnitude of $E_\parallel$. This is the standard case when the Polar spacecraft is in the cusp, where $f_{ce}<f_{pe}$. For the data in Fig. 3, $f_{ce}=3$ kHz and $f_{pe}=12.7$ kHz. The fact
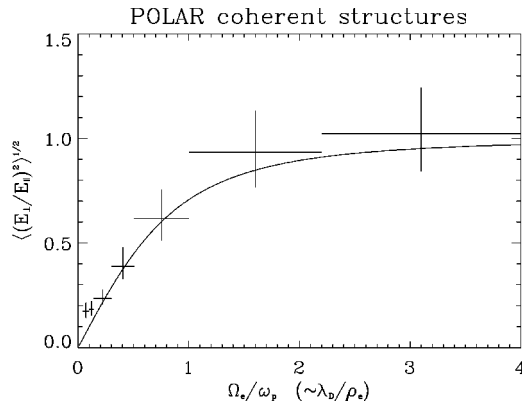
FIG. 4. $\langle (E_\perp/E_\parallel)^2 \rangle^{1/2} \propto L_\parallel/L_\perp$ vs Ω_e/ω_p. For these observations $T_{e\parallel} \simeq T_{e\perp}$, so $\Omega_e/\omega_p \approx \lambda_d/\rho_e$. From Franz *et al.*, Ref. 39, copyright by the American Geophysical Union. Used by permission of the American Geophysical Union.

that $E_\perp < E_\parallel$ suggests that structures are oblate with $L_\perp > L_\parallel$ ($L_\parallel$ is the scale size parallel to **B**, and $L_\perp$ is the scale size perpendicular to **B**). We will discuss this point in more detail below. The second feature in Fig. 3 is that the polarities of the perpendicular signatures are all the same. This feature suggests that the structures are somewhat spatially ordered in the perpendicular direction. The nature of this ordering is not yet understood.

One phenomenon consistent with the observations is the electron phase-space hole,[32] which is simply a depletion in the electron distribution function that is localized in both position space and velocity space. Particle trapping is required for such a structure, and therefore linear theory is not adequate to describe the electron holes. Electron phase-space holes, hereafter denoted by EH, were first observed in early simulations of electron beams in plasmas.[33] They were subsequently observed in the laboratory,[34] and it was determined that the larger amplitude structures tended to have larger scale sizes, just as we observe in space. EH have also been shown to be the fluctuation in a plasma that maximizes the entropy, given a fixed mass, momentum, and energy.[35]

Currently, there are only one-dimensional analytical models of EH.[36,37] While the Polar observations are consistent with those models,[38] the observations also clearly indicate that the EH are not one dimensional. However, the ratio of the measured peak electric fields, $E_\perp/E_\parallel$, may be used to estimate $L_\parallel/L_\perp$, since we expect $E_\perp/E_\parallel \propto \cos\alpha\, L_\parallel/L_\perp F(R_\perp/L_\perp)$. The $L_\parallel/L_\perp$ factor follows from the electrostatic nature of the phenomenon, and the $\cos\alpha$ factor is simply the result of only measuring one component of $\mathbf{E}_\perp$. $R_\perp$ is the perpendicular distance between the center of the EH and the spacecraft, and $F(R_\perp/L_\perp)$ depends upon the functional form of the electrostatic potential pulse. For each EH that is detected, neither α nor $R_\perp$ is known, so we consider them to be random variables. Therefore, we expect $\langle (E_\perp/E_\parallel)^2 \rangle^{1/2} \propto L_\parallel/L_\perp$.

We have analyzed over 1000 EH in a wide range of plasma environments with $0.04 \lesssim \Omega_e/\omega_p \lesssim 4$. For the Polar observations, $T_{e\parallel} \simeq T_{e\perp}$ so $\Omega_e/\omega_p \approx \lambda_d/\rho_e$. A plot of the estimated $\langle (E_\perp/E_\parallel)^2 \rangle^{1/2}$ versus Ω_e/ω_p is presented in Fig. 4.

Here we see that for $\Omega_e/\omega_p > 1$, the EH are roughly spherical. As Ω_e/ω_p gets smaller, the EH become more oblate with $L_\perp > L_\parallel$. This result is significant, as it is the only study (experimental, theoretical, or via simulations) of the scaling of EH oblateness with plasma parameters. A simple scaling argument[39] predicts $E_\perp/E_\parallel = L_\parallel/L_\perp = (1 + \omega_p^2/\Omega_e^2)^{-1/2}$, which is plotted as a solid line in Fig. 4. The trend in the Polar data is also consistent with other observations. In the auroral acceleration region where $5 < \Omega_e/\omega_p < 15$, $E_\perp \approx E_\parallel$;[31] in the geomagnetic tail where $\Omega_e/\omega_p \approx 0.2$, $E_\perp \approx 0$.[23] Finally, two-dimensional particle simulations with $\Omega_e/\omega_p = 5$ show that EH eventually evolve to a state with $E_\perp \approx E_\parallel$.[40]

IV. BROADBAND EXTRA LOW FREQUENCY ELECTRIC FIELDS AND TRANSVERSE ION ACCELERATION

Broadband extra low frequency (BB-ELF) electric fields have been established as the wave measurements most often associated with the most significant transverse ion acceleration (TIA) up to an altitude of at least 1700 km within the auroral ionosphere.[41] Because these fields are central to the wave-particle interactions producing TIA and, by extension, central to the ionosphere's contribution to magnetospheric mass, an understanding of the BB-ELF wave mode, its source of free energy, and how it produces TIA is required to understand the earth's magnetosphere and its weather.

The generally accepted definition of BB-ELF is fluctuating electric fields which appear random in the time domain and have a monotonically decreasing power spectrum from well below the O+ cyclotron frequency (30–35 Hz) to well above the H+ cyclotron frequency (500–600 Hz); that is, a few Hz to a few kHz. At the lowest frequencies, typically below the O+ cyclotron frequency, a magnetic component frequently accompanies the electric fields,[41] and the magnetic component amplitude typically decreases faster with frequency than the electric field amplitude. The broadband amplitudes are typically several mV/m to a few tens of mV/m. No one has reported any structure in the power spectrum at any of the cyclotron frequencies.

Sounding rocket experiments[6] have substantiated the result of André *et al.*[41] and have suggested some of the detailed properties of BB-ELF fields and their relation to TIA. The SCIFER (Sounding of the Cleft Ion Fountain Experimental Rocket) sounding rocket[42,43] demonstrated that BB-ELF was observed simultaneously with TIA contained in regions of ionospheric cavities. In another experiment (AMICIST: Auroral Microphysics Ion Conic Investigation In Space and Time),[44,45] Bonnell used a plasma wave interferometer to examine a relatively narrow region (20 km) of TIA and BB-ELF waves located in the most poleward nightside aurora before crossing into the polar cap. This work revealed that the BB-ELF waves in the frequency range of 200 Hz to 3 kHz had an upward phase velocity of 30–50 km/s, consistent with the thermal electron drift in field-aligned currents (FAC), and had finite values of $k_\parallel$ with typical $E_\perp$ to $E_\parallel$ ratios of 3–5. However, the implied FAC were stable in a homogeneous environment to the growth of electrostatic ion

cyclotron and ion acoustic waves.[46] In an effort to find a plausible normal mode which could explain these observations, Bonnell turned to electric field shear theories and laboratory experiments[47–49] which make the electrostatic hydrogen cyclotron mode unstable for the implied FAC.

The wavelength of BB-ELF electric fields is required to interpret this phenomenon. We will examine the coherency in the cross spectrum of the plasma wave interferometer data to infer wavelength. The condition that the coherency is large or close to one can be produced by a random distribution of independent wave vectors whose wavelengths are large compared to the interferometer length. When the coherency is small compared to one, the wavelength is bounded by a few times the interferometer length. A plasma wave interferometer consists of two spatially separated sensors—in this case, electric field sensors. The two sensors make two measurements in the time domain that we will call s_1 and s_2. If the Fourier transforms of s_1 and s_2 are S_1 and S_2, the cross spectrum becomes

$$C_{12} = \frac{\langle S_1 S_2^* \rangle}{\sqrt{\langle S_1^2 \rangle \langle S_2^2 \rangle}} = \gamma^2 e^{i\theta}, \tag{1}$$

where $\langle \ \rangle$ implies an ensemble average. The coherency spectrum (γ^2) is the magnitude of the frequency-dependent cross spectrum, and the phase spectrum θ is the phase of the cross spectrum. By Schwartz's inequality, the coherency must always be less than or equal to one. Coherency values near one can be produced by a random wave field whose wavelengths are all long compared to the interferometer sensor spacing, so that for all realizations, $I_M(S_1 S_2^*) = 0$. On the other hand, the coherency will be small when $I_M(S_1 S_2^*)$ is finite, implying that the wavelengths are the order of the interferometer length or smaller. This may be more apparent by seeing that each realization in the ensemble average produces a random number in the complex plane which, when averaged together, produces a small magnitude number. This implies a general relation in random, isotropic wave fields: long wavelengths produce large coherency and short wavelengths produce small coherency.

The PHAZE 2 (Physics of Auroral Zone Electrons) payload was launched into an active auroral display with transverse ion acceleration and BB-ELF electric field. The payload included an interferometer whose spin axis was aligned with the geomagnetic field and whose antenna extended perpendicular to the geomagnetic field. We can now examine a coherency function estimated by creating a single cross spectrum from the PHAZE 2 data from 380 to 540 s, a period when the BB-ELF had easily measured amplitudes and which was accompanied by TIA. Each FFT (fast Fourier transform) in the ensemble average is composed of 1600 points corresponding to 801 frequency bins with a frequency resolution of 25 Hz. The cross spectrum ensemble average is composed of 7889 realizations of 1600 data points. The PHAZE 2 cross spectrum up to 20 kHz and up to 2 kHz is shown in Fig. 5, along with the power spectrum for the same time interval. The upper panel of Fig. 5 shows a typical auroral hiss power spectrum (solid line) with a peak near the lower hybrid frequency at about 3 kHz and with structure at
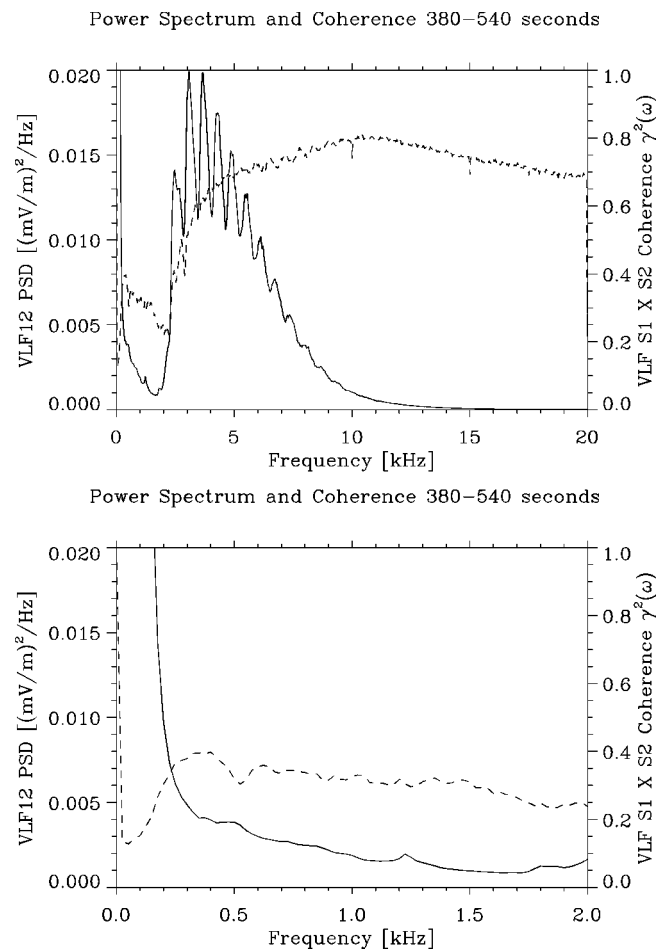

FIG. 5. The power spectrum (solid line, left-hand scale) and coherency spectrum (dashed line, right-hand scale) of broadband ELF electric fields observed simultaneously with transverse ion acceleration.

the H+ gyrofrequency typical of ion Bernstein modes.[50] The coherency spectrum (dashed line) is large above 5 kHz ($\gamma^2 \geq 0.6$), where the auroral hiss has a significant electromagnetic and long wavelength component. At and below the lower hybrid frequency, at 3 kHz the coherency becomes much smaller, corresponding to the short wavelengths at the lower hybrid resonance. In the lower panel the coherency and power spectra can be divided into two regimes. Above 400 Hz the spectral power is smaller and the coherency varies from 0.25 to 0.40. Below 400 Hz the power spectrum increases rapidly with decreasing frequency, but the coherency decreases from about 0.40 at 400 Hz to 0.15 at 25–50 Hz, which includes the O+ gyrofrequency. From a more detailed model of the coherency, we infer a range of possible wavelengths ranging from 30 to 10 m. For the O+ gyrofrequency at about 35 Hz, the 10 m wavelength implies a phase velocity of 350 m/s compared to the rocket velocity of about 1.2 km/s. These are extremely short wavelengths and slow phase velocities by space physics standards. The wavelengths are the order of the ion gyroradius, and the phase velocities are smaller than the ion acoustic velocity at the O+ gyrofrequency.

The very short wavelengths present in BB-ELF electric fields have several implications not previously considered.

First, the wavelength is much less than the electron skin depth of about 1 km, so these electric fields are clearly electrostatic. Given the implied electrostatic nature of these waves, it is not clear how to interpret the associated magnetic spectrum frequently associated with BB-ELF electric fields.[41] Second, the wavelengths are shorter than most satellite antenna lengths, implying that the wave electric fields have been underestimated, perhaps by as much as an order of magnitude. Third, the phase velocities at the O+ gyrofrequency are much less than rocket and satellite velocities, implying the existence of Doppler broadening. Hence, possible features in the rest frame, including nulls at the ion cyclotron frequencies, would not be observable.

Given these measurements, there are few normal modes available to choose from to explain the waves. For a homogeneous environment, there are only the ion acoustic or oblique ion acoustic modes (sometimes called the fast ion acoustic mode), the slow ion acoustic mode, the electrostatic ion cyclotron modes, and inertial Alfvén waves. The ion acoustic modes should not exist unless $T_e \gg T_i$, which is not the case. The ion cyclotron mode at the H+ gyrofrequency has spectral features ordered by the gyrofrequency, which should be observable from sounding rockets despite the Doppler broadening, and they are not. At the O+ gyrofrequency, the phase velocity should be several times the ion thermal velocity, and we estimate a phase velocity less than the ion thermal velocity. Thus the homogeneous oblique ion acoustic and electrostatic ion cyclotron modes can be eliminated.

The slow ion acoustic mode, characterized by nearly perpendicular propagation and short wavelengths, has been investigated by Seyler and Wahlund[51] and Wahlund et al.[52] as a source of BB-ELF waves. This mode agrees with the wavelength measurements represented herein and does not require that $T_e \gg T_i$, but does require $T_e \ll T_i$. Further, it admits a measurable magnetic field in its dispersion relation. However, the slow ion acoustic mode implies that there should be no parallel electric fields associated with BB-ELF, which does not agree with either AMICIST or PHAZE 2 measurements. Another candidate for BB-ELF electric fields is inertial Alfvén waves. Stasiewicz et al.[53] have investigated this mode, including finite ion gyroradius corrections. They predict nearly perpendicular propagation and wavelengths of 30 to 7000 m. Only the very shortest wavelengths agree with our investigation, and the prediction of no significant parallel electric fields disagrees with AMICIST and PHAZE 2 measurements.

Several inhomogeneous modes have been examined for the frequency range of BB-ELF waves. Bonnell[45] has suggested that the velocity shear-assisted modes, sometimes called the inhomogeneous energy-density-driven (IEDD) instability,[47,49,54–57] are responsible for the BB-ELF electric fields observed by AMICIST. The advantage of this mode is that the ordering of spectral features by the gyrofrequencies is ''smeared out,'' leaving a broadband spectrum, as observed, if adequate transverse velocity shear is present. Another promising hypothesis has been developed by Gavrishchaka et al.,[58,59] suggesting that ion acoustic modes can exist for all T_e/T_i ratios if there is shear in the parallel plasma drift. Unfortunately, we do not yet have the capability to test

this hypothesis, but hopefully, laboratory experiments will explore this path. The source of free energy for BB-ELF electric fields remains unknown. Although generally found in active auroral regions, they do not correlate with precipitating electrons or large amplitude, higher frequency electric fields. There is some correlation with field-aligned currents as measured by magnetometers,[41,60–62] suggesting that parallel electron drift is the source of free energy. This hypothesis is consistent with the SCIFER results that BB-ELF electric fields were closely correlated with regions of lower electron density where electrons must drift faster to carry the same current. Measurement of parallel electron drift or parallel plasma drift in regions of TIA and BB-ELF electric fields has never been accomplished with sufficient resolution to detect field-aligned currents or significant shears and should be a high priority for future experiments.

V. CONCLUSIONS

Our understanding of waves in space plasmas has benefitted during the past decade from two significant instrumental advances. The first advance is the development of plasma wave receivers with spatially separated electric field antennae called plasma wave interferometers, and the second advance is the use of higher bandwidth telemetry systems or snapshot receivers to capture wave forms of plasma wave data. The first development has led to the understanding of wavelength, propagation direction, and propagation speed of phenomena whose existence has been known for decades, but for which there has been no adequate physical explanation. The second development has revealed the structure of nonlinear phenomena, such as electron phase-space holes, which may have near-universal significance in space plasmas. For example, it may explain the majority of broadband electrostatic noise,[63] which has eluded explanation for more than two decades.

The three examples presented here are a sample of the progress made possible when multipoint measurements are combined with full wave form data, even if the data are in snapshot form. With the promise of several planned new experiments using multiple spacecraft instead of just multiple sensors, we should expect similar progress in understanding space plasmas.

ACKNOWLEDGMENTS

[1] J. LaBelle and P. M. Kintner, Rev. Geophys. **27**, 495 (1989).
[2] J. Labelle, P. M. Kintner, A. W. Yau, and B. A. Whalen, J. Geophys. Res. **91**, 7113 (1986).
[3] R. Arnoldy, K. Lynch, P. M. Kintner, J. Vago, S. Chesney, T. E. Moore, and C. J. Pollock, Geophys. Res. Lett. **19**, 413 (1992).
[4] P. M. Kintner, J. Vago, S. Chesney, R. L. Arnoldy, K. A. Lynch, C. J. Pollock, and T. E. Moore, Phys. Rev. Lett. **68**, 2448 (1992).
[5] J. L. Vago, P. M. Kintner, S. W. Chesney, R. L. Arnoldy, K. A. Lynch, T.

E. Moore, and C. J. Pollock. J. Geophys. Res. **97**, 16 935 (1992).

[6] K. A. Lynch, R. L. Arnoldy, P. M. Kintner, and J. Bonnell, Geophys. Res. Lett. **23**, 3293 (1996).

[7] G. T. Delory, Ph.D. thesis, University of California at Berkeley, 1996.

[8] G. T. Delory, R. E. Ergun, E. M. Klementis, C. W. Carlson, and J. P. McFadden, Geophys. Res. Lett. **24**, 1131 (1997).

[9] J.-L. Pinçon, P. M. Kintner, P. W. Schuck, and C. E. Seyler, J. Geophys. Res. **102**, 17 283 (1997).

[10] P. W. Schuck, C. E. Seyler, J.-L. Pinçon, J. W. Bonnell, and P. M. Kintner, J. Geophys. Res. **103**, 6935 (1998).

[11] J. W. Bonnell, P. W. Schuck, J.-L. Pinçon, C. E. Seyler, and P. M. Kintner, Phys. Rev. Lett. **80**, 5734 (1998).

[12] K. A. Lynch, R. L. Arnoldy, P. M. Kintner, P. W. Schuck, J. W. Bonnell, and V. N. Coffey, J. Geophys. Res. **104**, 28 515 (1999).

[13] P. O. Dovner, A. I. Eriksson, R. Boström, and B. Holback, Geophys. Res. Lett. **21**, 1827 (1994).

[14] A. I. Eriksson, B. Holback, P. O. Dovner *et al.*, Geophys. Res. Lett. **21**, 1843 (1994).

[15] P. O. Dovner, A. I. E. R. Boström, and B. Holback, Geophys. Res. Lett. **24**, 619 (1997).

[16] H. L. Pécseli, K. Iranpour, O. Holter *et al.*, J. Geophys. Res. **101**, 5299 (1996).

[17] H. L. Pécseli, B. Lybekk, J. Trulsen, and A. Eriksson, Plasma Phys. Controlled Fusion **39**, A277 (1997).

[18] D. J. Knudsen, J. H. Clemmons, and J.-E. Wahlund, J. Geophys. Res. **103**, 4171 (1998).

[19] S. H. Kjus, H. L. Pécseli, B. Lybekk, J. Holtet, J. Trulsen, H. Lühr, and A. Eriksson, J. Geophys. Res. **103**, 26 633 (1998).

[20] D. A. Gurnett, A. M. Persoon, R. F. Randall *et al.*, Space Sci. Rev. **71**, 597 (1995).

[21] J. R. Franz, P. M. Kintner, and J. S. Pickett, Geophys. Res. Lett. **25**, 1277 (1998).

[22] C. Cattell, J. Wygant, J. Dombeck, F. S. Mozer, M. Temerin, and C. T. Russell, Geophys. Res. Lett. **25**, 857 (1998).

[23] H. Matsumoto, H. Kojima, T. Miyatake, Y. Omura, M. Okada, I. Nagano, and M. Tsutsui, Geophys. Res. Lett. **21**, 2915 (1994).

[24] H. Kojima, H. Matsumoto, S. Chikuba, S. Horiyama, M. Ashur-Abdalla, and R. R. Anderson, J. Geophys. Res. **102**, 14 439 (1997).

[25] H. Matsumoto, H. Kojima, Y. Kasaba, T. Miyatake, R. R. Anderson, and T. Mukai, Adv. Space Res. **20**, 683 (1997).

[26] S. D. Bale, P. J. Kellogg, D. E. Larson, R. P. Lin, K. Goetz, and R. P. Lepping, Geophys. Res. Lett. **25**, 2929 (1998).

[27] A. Mangeney, C. Salem, C. Lacombe *et al.*, Ann. Geophys. **17**, 307 (1999).

[28] F. S. Mozer, R. Ergun, M. Temerin, C. Cattell, J. Dombeck, and J. Wygant, Phys. Rev. Lett. **79**, 1281 (1997).

[29] R. E. Ergun, C. W. Carlson, J. P. McFadden *et al.*, Geophys. Res. Lett. **25**, 2025 (1998).

[30] R. E. Ergun, C. W. Carlson, J. P. McFadden *et al.*, Geophys. Res. Lett. **25**, 2041 (1998).

[31] R. E. Ergun, C. W. Carlson, J. P. McFadden, F. S. Mozer, L. Muschietti, I. Roth, and R. Strangeway, Phys. Rev. Lett. **81**, 826 (1998).

[32] H. Schamel, Phys. Scr. **20**, 336 (1979).

[33] K. V. Roberts and H. L. Berk, Phys. Rev. Lett. **19**, 297 (1967).

[34] K. Saeki, P. Michelsen, H. L. Pécseli, and J. J. Rasmussen, Phys. Rev. Lett. **42**, 501 (1979).

[35] T. H. Dupree, Phys. Fluids **25**, 277 (1982).

[36] V. L. Krasovsky, H. Matsumoto, and Y. Omura, J. Geophys. Res. **102**, 22 131 (1997).

[37] L. Muschietti, R. E. Ergun, I. Roth, and C. Carlson, Geophys. Res. Lett. **26**, 1093 (1999).

[38] J. R. Franz, Ph.D. thesis, Cornell University, Ithaca, New York, 2000.

[39] J. R. Franz, P. M. Kintner, C. E. Seyler, J. S. Pickett, and J. D. Scudder, Geophys. Res. Lett. **27**, 169 (2000).

[40] M. V. Goldman, M. M. Oppenheim, and D. L. Newman, Geophys. Res. Lett. **26**, 1821 (1999).

[41] M. André, P. Norqvist, L. Andersson *et al.*, J. Geophys. Res. **103**, 4199 (1998).

[42] P. M. Kintner, J. Bonnell, R. Arnoldy *et al.*, Geophys. Res. Lett. **23**, 1865 (1996).

[43] P. M. Kintner, J. Bonnell, R. Arnoldy, K. Lynch, C. Pollock, and T. Moore, Geophys. Res. Lett. **23**, 1873 (1996).

[44] J. Bonnell, P. Kintner, J.-E. Wahlund, K. Lynch, and R. Arnoldy, Geophys. Res. Lett. **23**, 3297 (1996).

[45] J. W. Bonnell, Ph.D. thesis, Cornell University, Ithaca, New York, 1997.

[46] J. M. Kindel and C. F. Kennel, J. Geophys. Res. **76**, 3055 (1971).

[47] G. Ganguli and P. Palmadesso, Geophys. Res. Lett. **15**, 103 (1988).

[48] M. E. Koepke, W. E. Amatucci, J. J. Carroll III, V. Gavrishchaka, and G. Ganguli, Phys. Plasmas **2**, 2523 (1995).

[49] W. E. Amatucci, D. N. Walker, G. Ganguli *et al.*, J. Geophys. Res. **103**, 11 711 (1998).

[50] P. Kintner, W. Scales, J. Vago, A. Yau, B. Whalen, R. Arnoldy, and T. Moore, J. Geophys. Res. **96**, 9627 (1991).

[51] C. E. Seyler and J. E. Wahlund, J. Geophys. Res. **101**, 795 (1996).

[52] J.-E. Wahlund, A. I. Eriksson, B. Holback *et al.*, J. Geophys. Res. **103**, 4343 (1998).

[53] K. Stasiewicz, Y. Khotyaintsev, M. Berthomier, and J.-E. Wahlund, Geophys. Res. Lett. **27**, 173 (2000).

[54] M. Koepke, W. Amatucci, J. J. Carroll III, V. Gavrishchaka, and G. Ganguli, Phys. Plasmas **2**, 2523 (1995).

[55] J. J. Carroll III, M. Koepke, M. Zintl, V. Gavrishchaka, and G. Ganguli, Geophys. Res. Lett. **25**, 3099 (1998).

[56] M. Koepke, J. J. Carroll III, and M. Zintl, J. Geophys. Res. **104**, 14 397 (1999).

[57] D. Walker, W. Amatucci, G. Ganguli *et al.*, Geophys. Res. Lett. **24**, 1187 (1997).

[58] V. Gavrishchaka, S. Ganguli, and G. Ganguli, Phys. Rev. Lett. **80**, 728 (1998).

[59] V. Gavrishchaka, S. Ganguli, and G. Ganguli, J. Geophys. Res. **104**, 12 683 (1999).

[60] P. Norqvist, M. André, L. Eliasson, A. Eriksson, L. Blomberg, H. Lühr, and J. Clemmons, J. Geophys. Res. **101**, 13 179 (1996).

[61] M. H. Boehm, personal communication, 1998.

[62] J. Bonnell, personal communication, 1999.

[63] D. A. Gurnett and L. A. Frank, J. Geophys. Res. **82**, 1031 (1977).